J Mater Sci (2022) 57:1962–1976

Energy materials

Cellulose/Ag-MWCNT/MXene composite scaffolds with hierarchical pores and fast light-to-heat conversion for the preparation of shape-stable phase change materials for thermal energy storage

Qian Wang[1], Zhuan Gao[1], and Yuzhu Xiong[1,*]

[1] *Department of Polymer Materials and Engineering, College of Materials and Metallurgy, Guizhou University, Guiyang 550025, China*

Received: 17 September 2021
Accepted: 22 October 2021
Published online: 3 January 2022

ABSTRACT

Due to the global energy crisis, it is urgently necessary to improve the efficiency of traditional energy utilization and develop renewable energy sources to achieve sustainable energy development. Herein, composite scaffolds with hierarchical pores and fast light-to-heat conversion were prepared for thermal energy storage to address the intermittency problem of renewable energy sources. Microcrystalline cellulose (MCC), MXene, and silver-loaded multi-walled carbon nanotubes (Ag-MWCNT) were cross-linked to prepare a three-dimensional network composite hydrogel. A porous structure of the MCC/Ag-MWCNT/MXene (Ag-MMCT) composite scaffolds were obtained via the cryodesiccation method, and the assisted vacuum impregnation method was used to absorb palmitic acid (PA) and prepare MCC/Ag-MWCNT/MXene/PA (Ag-PMMCT) composite phase change materials. The Ag-MMCT composite scaffold exhibited a typical hierarchical pores structure that provided suitable space for PA packaging, and the interpenetrating network structure scaffolds formed an effective thermal conduction network. As a result, the Ag-PMMCT composite phase change material exhibited excellent encapsulation and shape stability. Furthermore, Ag-PMMCT composite phase change materials showed high latent heat (153.8 J g^{-1}) and fast light-to-heat energy conversion capability, with the phase transition under light irradiation occurring after 223 s of irradiation. In particular, for the MXene to Ag-MWCNT ratio of 1:1, the thermal conductivity of the composite phase change material was 0.653 $W{\cdot}m^{-1}$ K^{-1}, corresponding to an increase of 202.3% relative to that of pure PA. Overall, the Ag-PMMCT composite phase change materials show great potential for

Handling Editor: Stephen Eichhorn.

Address correspondence to E-mail: xyzhu789@126.com

https://doi.org/10.1007/s10853-021-06659-7

applications in energy conversion and storage systems and in thermal management of devices and electronics.

GRAPHICAL ABSTRACT

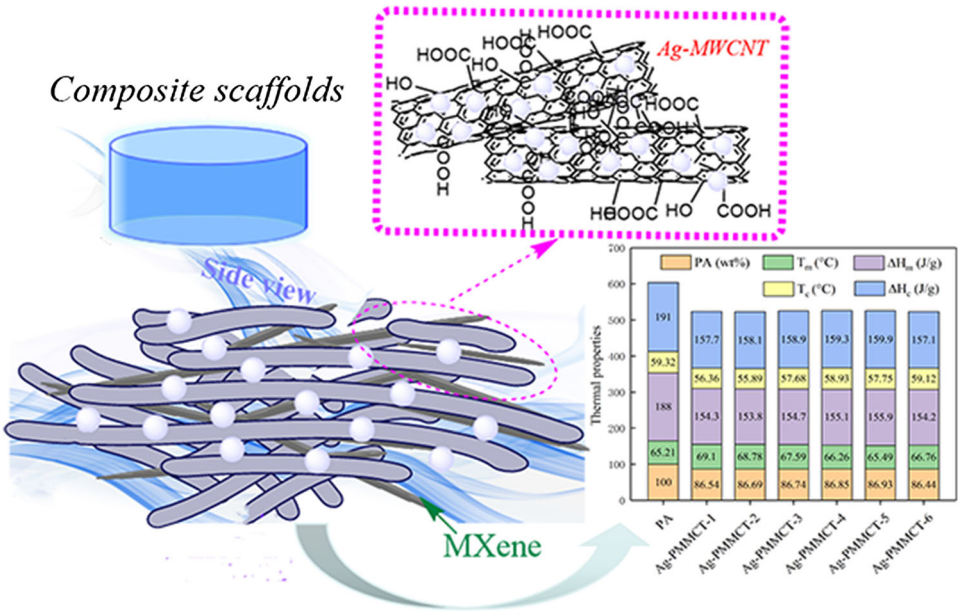

Introduction

With the increasingly severe energy crisis, improving the efficiency of traditional energy utilization and the development of various renewable energy sources have become major strategic goals in the global effort to achieve sustainable energy development [1]. Renewable energy sources such as solar energy and geothermal energy have the advantages of essentially unlimited reserves and environmental friendliness. In particular, solar energy is considered to be the most promising renewable energy source. The annual solar radiation energy obtained by the Earth is equivalent to 15,000 times the total annual energy consumption every year and approximately two-thirds of China's annual solar radiation energy. The annual illumination duration of over 2000 h provides good conditions for the development of solar energy utilization in China [2]. While it is clear that renewable energy is favored by its long-term accessibility and environmental friendliness, its intermittent energy supply, and intensity instability limit its applications. Thermal storage technology can be used for controllable collection, storage, and release of thermal energy. The use of thermal storage technology is an effective approach to improve energy utilization efficiency and has attracted intense research attention [3–7]. Thus, it is urgently necessary to develop thermal storage systems with good thermal storage properties for the collection, storage, and release of solar thermal energy to enable better utilization of solar energy resources.

Phase transition materials (PCMs) are a class of organic or inorganic compounds that can absorb, store, and release significant heat energy during a phase transition and form the basis for phase change energy storage devices [8]. The storage and release process occurs near the phase transition point and is an isothermal or approximately isothermal process. In recent years, due to their high energy storage density and good prospects for application in the field of energy storage, PCMs have attracted much research attention [9]. There are many types of PCMs

that can be categorized as solid–solid, solid–liquid, solid–gas, and liquid–gas materials according to the phase transition mechanism [10]. Organic solid–liquid phase transition materials [11, 12] have the advantages of good molding, non-toxicity, lack of corrosion, good compatibility, and almost no overcooling and phase separation during the phase change process [13]. Among these materials, polyethylene glycol and palmitic acid not only have the advantages of common organic phase change materials, but are also green and renewable materials, meeting a common goal of contemporary research efforts [14]. However, organic solid–liquid phase change materials have the disadvantages of low thermal conductivity and easy leakage of the liquid phase during the phase change process. Therefore, enhancing the thermal conductivity of organic solid–liquid phase change materials and preventing leakage are key tasks for enabling the use of these materials in practical applications.

Carbon-based materials, such as expanded graphite (EG), carbon fiber (CF), graphene, and carbon nanotubes (CNT) [15, 16] have become some of the most popular additives in phase change composite materials due to their high thermal conductivity, stable chemical properties, wide availability and low density [17]. Silane coupling agent grafted CNT/PA phase change composite thermal storage materials [18], paraffin/diatomite/MWCNT composite phase change materials [19], and core–shell structure of CNT/stearyl alcohol/urea resin/paraffin micro-capsule phase change materials [20] are some examples of these materials. The two-dimensional transition metal carbon–nitrogen hybrid MXenes have recently received much attention in the fields of electromagnetic shielding and supercapacitors due to their excellent electromagnetic wave absorption capability and conductivity [21–23]. Compared to carbon materials, MXenes exhibit an apparent light absorption enhancement due to the local surface plasmon resonance (LSPR) effect [24, 25]. Furthermore, MXenes exhibit excellent light absorption in the visible and near-infrared regions, significantly improving the solar-thermal conversion efficiency of PCM composites [26, 27]. Tang et al. [28] encapsulated polyethylene glycol in MXene/bacterial cellulose porous aerogel to prepare composite phase change materials that exhibited good light-to-heat conversion capabilities.

Herein, we report MCC/Ag-MWCNT/MXene composite scaffolds with hierarchical pores and fast light-to-heat conversion that are used to prepare a shape-stable phase change material for thermal energy storage. Exploiting the synergy between the two-dimensional MXene with excellent light-to-heat conversion ability and Ag-MWCNT, the aqueous blend of MCC, MXene, and Ag-MWCNT was cross-linked to prepare a composite hydrogel that was freeze-dried to obtain porous Ag-MMCT composite scaffolds. The Ag-PMMCT composite phase change material was prepared via the vacuum impregnation method for absorption of PA. The effects of MXene addition on the pore structure of the Ag-MMCT composite scaffolds, and the thermal conductivity and light-to-heat conversion of the Ag-PMMCT composite phase change material were investigated. Overall, Ag-PMMCT composite phase change materials are promising for applications in solar thermal utilization, energy conversion and storage systems, and thermal management of equipment and electronic devices. Simultaneously, this approach provides a new strategy for the practical application of palmitic acid in the field of solar thermal utilization.

Materials and methods

Materials

Ti_3AlC_2 (99.99%) was purchased from Jilin 11 Technology Co., Ltd. Lithium fluoride (LiF, 99.9%), lithium hydroxide (LiOH, 99.9%), urea (≥ 99.5%), epichlorohydrin (ECH, 99.9%), sodium citrate (AR), dimethyl sulfoxide (DMSO, 99.9%), and palmitic acid (PA, AR) were obtained from Shanghai Bio-Chem Technology Co., Ltd. Microcrystalline cellulose (MCC, M_w: $(162.02)_n$) was obtained from Cuer Bioengineering Co., Ltd. Silver nitrate ($AgNO_3$, AR) was provided from Sinopharm Chemical Reagent Co., Ltd. Multi-walled carbon nanotubes (MWCNT, > 98wt%) was provided from Zhongke Timesnano Co., Ltd. Nitric acid (HNO_3, AR), potassium permanganate ($KMnO_4$, AR), sulfuric acid (H_2SO_4, AR), and hydrochloric acid (HCl, AR) were provided from Chongqing Chuandong Chemical (Group) Co., Ltd. Distilled water was prepared in the laboratory using a Milli-Q water system.

Preparation of Ag-MWCNT

Ag-MWCNT preparation was carried out as follows. MWCNTs were purified according to the method

reported by Chiang et al. [29], and then, high-temperature oxidation was carried out by adding the purified MWCNTs to a mixed $KMnO_4/H_2SO_4$ solution. Next, Ag-MWCNTs were prepared by the dimethyl sulfoxide (DMSO) reduction method to obtain in-situ loaded silver nanoparticles on the surface of the MWCNTs [30].

Preparation of MXene nanosheets

First, LiF powder (1.16 g) was dissolved in an HF solution (9 mol/L, 20 mL). Second, Ti_3AlC_2 (1 g) was slowly added to the mixed LiF/HCl solution with stirring and then etched at 35 °C for 24 h. After the reaction, the precipitates were washed to pH > 6 by centrifugation with abundant distilled water to obtain multilayer MXenes. Next, the multilayer MXenes were dispersed in distilled water (100 mL) and ultrasonically stripped for 1 h, and then the dispersion solution was centrifuged at 3500 rpm for 1 h. Finally, the supernatant was freeze-dried to obtain few-layer MXene nanosheets.

Preparation of Ag-MMCT composite scaffolds

MCC powder (1.8 g) was dissolved in a mixed LiOH/urea solution with the mass ratio of LiOH, urea, and H_2O of 0.46:1.5:8.04. Next, certain amounts of Ag-MWCNT and MXene were added to the mixture to obtain a uniformly dispersed suspension and then the suspension was transferred to the refrigerator to freeze overnight at −12 °C. After thawing, the suspension was placed in an ice-water bath, and then a small amount of ECH was added dropwise with stirring. After vacuum degassing, the mold was installed, and then reacted in an oven at 60 °C for 3 h to obtain MCC/Ag-MWCNT/MXene composite hydrogels. Finally, the as-prepared composite hydrogels were washed with distilled water to remove the unreacted reductants from the hydrogel matrix, and then were freeze-dried to obtain composite scaffolds with a three-dimensional porous structure. The as-prepared composite scaffolds are denoted as Ag-MMCT-X according to their MXene content, with X = 1, 2, 3, 4, 5, and 6, respectively, representing the MXene contents of 0.18, 0.36, 0.54, 0.72, 0.9, and 1.08 g (Table S1).

Preparation of Ag-PMMCT composite phase change materials

The Ag-PMMCT composite phase change material was prepared through the absorption of PA into the composite scaffold by the vacuum impregnation method. An appropriate amount of PA was fully melted in the vacuum oven of 80 °C, and the Ag-MMCT scaffold was immersed into the melted PA. Then, a vacuum pump was used to degas for 5 min and a steady state was maintained for 30 min. This process was repeated for 12 h to ensure that the scaffold was completely filled with PA, and then the impregnated PA scaffold was removed and cooled to room temperature to obtain the Ag-PMMCT composite phase change material. The as-prepared composite phase change materials are denoted as Ag-PMMCT-X according to their MXene contents, with X = 1, 2, 3, 4, 5, and 6 representing the MXene contents of 0.18, 0.36, 0.54, 0.72, 0.9, and 1.08 g, respectively.

Physicochemical characterization of composites and the composite phase change material

Atomic force microscopy (AFM) was performed using a Bruker Dimension ICON type atomic force microscope (Bruker, USA) to analyze the morphology and thickness of the prepared MXene. The working voltage was 220 V, and the resolution was 1.5 μm. Fourier-transform infrared (FTIR) spectroscopy was performed using a Thermo Nicolet iS50 instrument to analyze the chemical structure of the Ag-PMMCT composite phase change material. X-ray photoelectron spectroscopy (XPS) with a monochromatic Al Kα X-ray source was used to analyze the elemental compositions of the composites (Thermo Fisher Scientific, USA). X-ray diffraction (XRD) was performed using an Empyrean sharp-shadow X-ray diffractometer to analyze the crystallization ability of the Ag-PMMCT composite phase change materials in the 2θ scanning range of 5–90°, with the scanning speed of 10° min^{-1}. Differential scanning calorimetry (DSC) measurements were carried out under nitrogen flow using a TA AQ20 instrument in the temperature range of 0–100 °C at a heating rate of 10 °C min^{-1}. For all of the samples, the thermal stability was analyzed using a thermogravimetric apparatus (TG209F1LIbrahin, Germany) at the temperature

ranging from the ambient temperature to 800 °C under nitrogen flow at a heating rate of 10 °C min^{-1}. The morphologies of Ag-MMCT and Ag-PMMCT were observed by scanning electron microscopy (SEM, HITACHI SU8010, Hitachi, Japan), the samples were treated with liquid nitrogen brittle fracture, and all samples were treated with gold spraying. The optical absorption capacity of the samples was evaluated by UV–vis-NIR spectrometer equipped. The specific surface areas and pore size distributions of the scaffolds were studied by Brunauer–Emmett–Teller (BET) method.

Thermal conductivity of composite phase change materials

The thermal conductivity of the Ag-PMMCT composite phase change material was measured using a laser thermal conductivity meter at room temperature. Each sample was cold pressed at 10 MPa to form a square sample with a side length of 10 mm and a thickness of 1.5 mm. Three points were tested for each sample, and the average value was taken.

Shape stability of composite phase change materials

The shape stability of the composite phase change material was analyzed by placing the Ag-PMMCT composite phase change material under a heating plate for continuous heating at 70 °C and obtaining photographs of the materials at different times. Then, the shape change and leakage of the Ag-PMMCT composite phase change material was analyzed.

Light-to-heat conversion of composite phase change materials

The photothermal conversion experiments of the composite phase change materials were carried out by placing the samples under a xenon lamp (BBZM-I) with an intensity of 100 mW cm^{-2}. The samples were irradiated for 900 s at ambient temperature with an irradiation distance of 10 cm between the sample and the bulb. After the irradiation, the samples were cooled for 1500 s. The variation of the temperature was recorded using a thermocouple paperless recorder (OMEGA). The photothermal conversion efficiency was calculated according to the following equation [31]:

$$\eta = \frac{m \times \Delta H}{A \times P \times t} \quad (1)$$

where m is the mass, ΔH is phase change enthalpy, A is exposed surface area of the sample, P is the power ($w \cdot cm^{-2}$) of irradiation light, and t is the time taken for the phase transition.

Results and discussion

Morphology and chemical structure of MXene nanosheets

MXene nanosheets were selectively etched using mixed LiF/HCl solutions and ultrasonic stripping stratification [32]. The etched MXene nanosheets are loose and a dark green dispersion is obtained after a simple ultrasonic treatment. To explore the structure of the resulting MXene nanosheets, AFM characterization was performed with the results shown in Fig. 1a–c. The thickness of the as-prepared MXene nanosheets was 1.6–2.3 nm and the nanosheets were either single- or double-layer MXene nanosheets. Using green laser irradiation, a clear green light pathway appears (Fig. 1d), which is typical of the Dindar effect, indicating that the MXene nanosheets were evenly dispersed in the water.

To further explore the etching of the aluminum (Al) layer in Ti_3AlC_2, the MXene structure was characterized by XRD. The characteristic diffraction peaks of Ti_3AlC_2 are observed in the XRD spectral graph (Fig. 1e) and correspond to the six-square structure [33]. In the MXene spectrum, the characteristic Al (104) peak disappears, and the characteristic (002) peak shifts from 9.50° to 7.07°, indicating that the insertion of Li^+ increases the layer spacing of the MXene [34]. The etching of Ti_3AlC_2 was further explored by XPS spectroscopy (Fig. 1f). The F, O, Ti, and C elements were observed on the surface of MXene nanosheets and the vanishing signal of Al elements proved that the etching was successful, indicating that few-layer MXene nanosheets can be successfully prepared through etching and ultrasonic stripping. Furthermore, MXene nanosheets contain a large number of hydrophilic groups, such as the –O, –OH, and –F groups, endowing MXenes with excellent water dispersibility. These groups are also beneficial for the preparation of MXene-based composite materials.

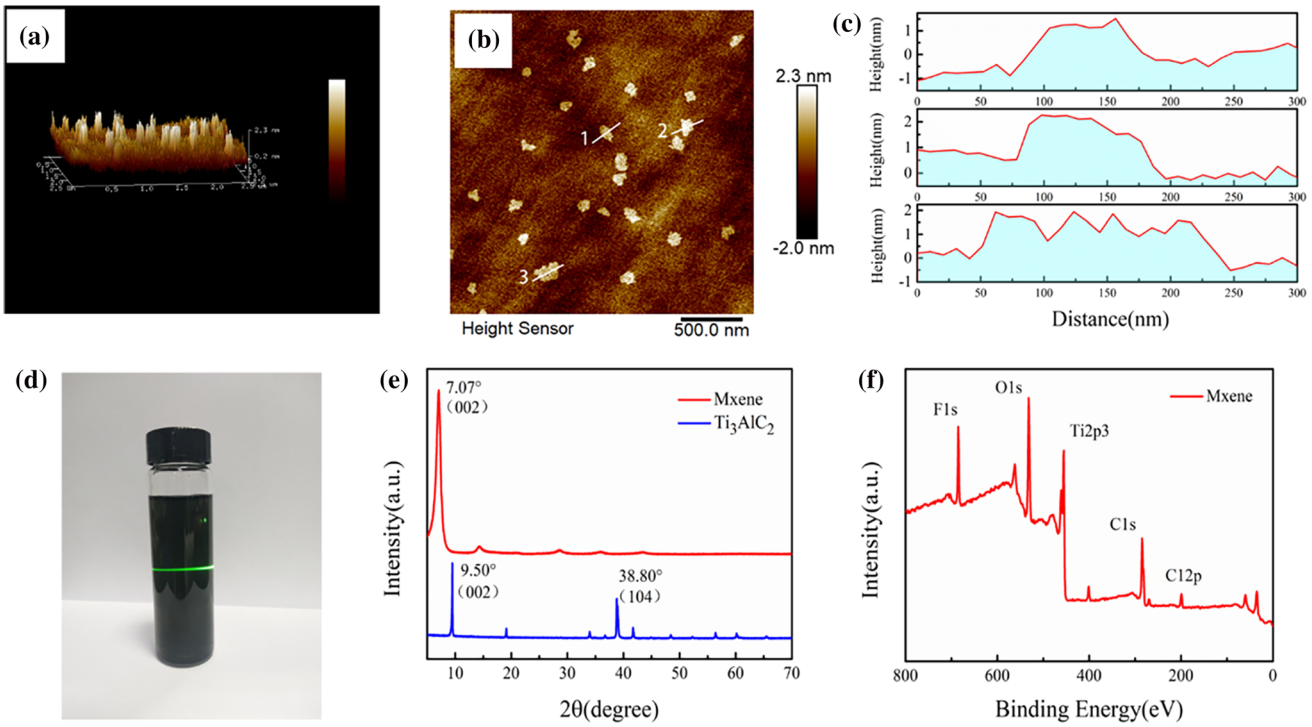

Figure 1 Morphology of MXene nanosheets (**a-c**), the dispersion of MXene aqueous solution (**d**), XRD spectrum (**e**) and XPS spectrum (**f**) of MXene nanosheets.

Morphology of Ag-MMCT composite scaffolds

Porous media phase change composite materials use the capillary force and surface tension of the porous media micropores to firmly confine the phase change material in the micropores, hindering its leakage even when the phase change material undergoes a phase transition. The preparation of the MCC/Ag-MWCNT/MXene composite scaffold with hierarchical pore structure and rapid photothermal conversion is shown in Fig. 2. The aqueous blend of MCC, Ag-MWCNT, and MXene was chemically cross-linked by ECH to obtain a composite hydrogel, and then the Ag-MMCT composite scaffold with a three-

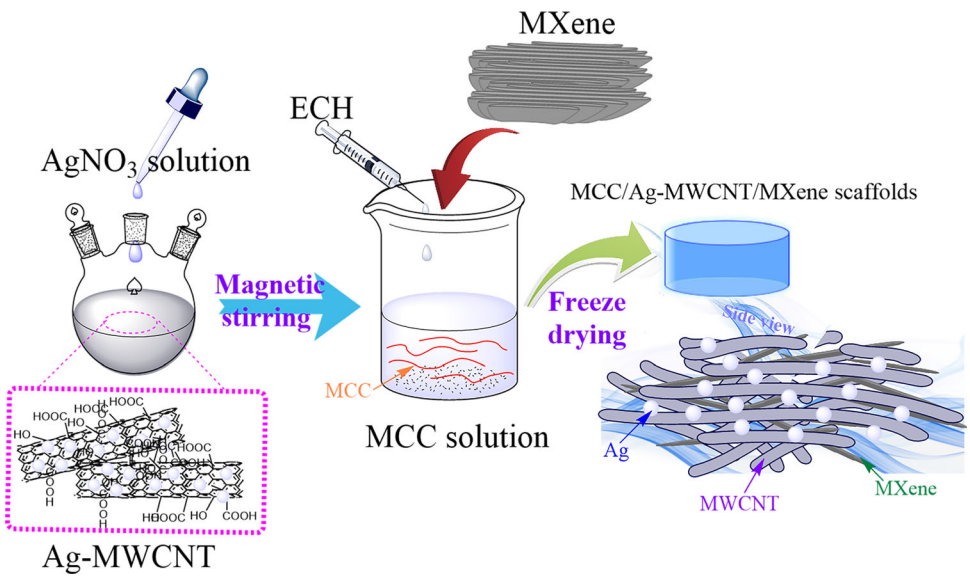

Figure 2 Schematic illustration of the preparation of MCC/Ag-MWCNT/MXene composite scaffolds.

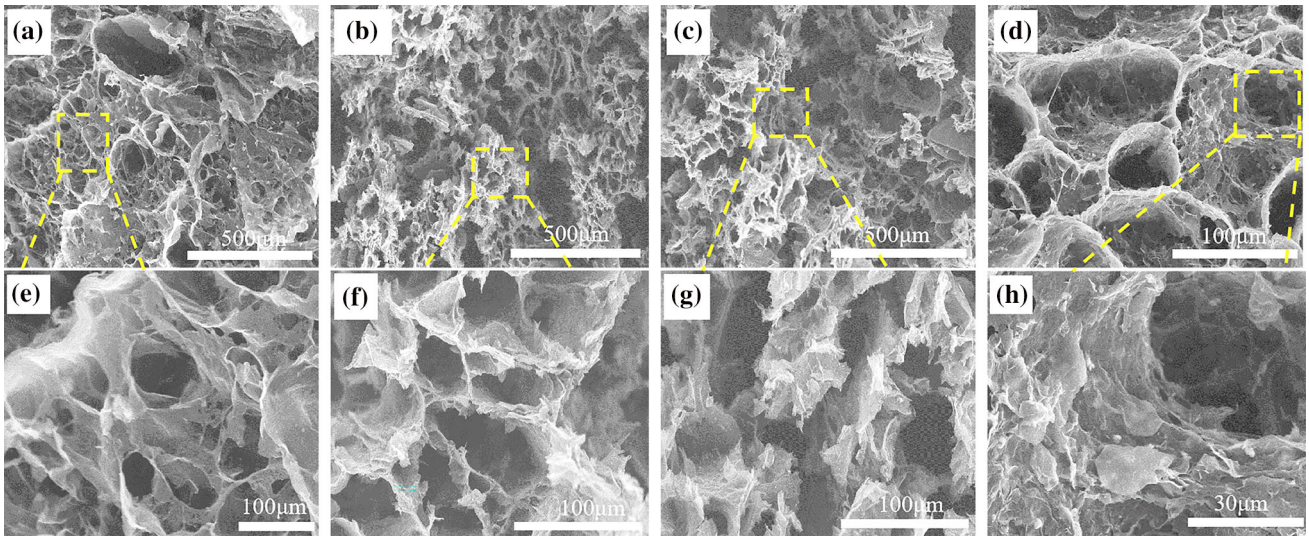

Figure 3 **a–d** SEM images of Ag-MMCT-1, Ag-MMCT-3, Ag-MMCT-5 and Ag-MMCT-6, respectively. The corresponding enlarged SEM images (**e**, **f**, **g** and **h**).

dimensional porous structure was prepared via the cryodesiccation method.

All of the Ag-MMCT scaffolds exhibited a typical hierarchical pore structure that provided good adsorption and packaging space for PA and effectively prevents PA leakage during the phase change process (Fig. 3). The interpenetrated three-dimensional network structure of the composite scaffolds formed good thermal conduction paths that give rise to the enhanced thermal conductivity of PA. For the MXene content below 21.5 wt%, as the MXene content increases, the pore structure of the Ag-MMCT framework tends to be uniform (Fig. 3a–c). When the MXene content reaches 21.5 wt%, the macropores in the hierarchical pore structure of the framework increase (Fig. 3d). This is because the synergistic interaction between the one-dimensional structure of Ag-MWCNT and the two-dimensional structure of MXene is beneficial for the formation of pores [35]. It was found that excessive MXenes cannot be completely covered by the Ag-MMCT framework and are exposed (Fig. 3h).

Morphology of Ag-PMMCT composite phase change materials

The cross-sectional morphology of the Ag-PMMCT composite phase change materials is shown in Fig. 4. No obvious cavities were found in the SEM images of all of the composite phase change materials, indicating that the vacuum impregnation method is effective, and PA was fully filled into the interior of the skeleton. Vacuum impregnation escapes the gas in the composite scaffolds to form the gap and channel, thus facilitating the infiltration and diffusion of PA. Moreover, the local magnified images of Ag-PMMCT-1, Ag-PMMCT-3, and Ag-PMMCT-5 composite phase change materials demonstrated that there was almost no phase separation between PA and the skeleton, indicating the excellent interface compatibility between the composite skeleton and PA (Fig. 4d–f). This is beneficial for reducing the interface thermal resistance of the composite phase change material in the heat transfer process and enhancing the thermal conductivity [36].

Chemical structure and crystallization capacity of Ag-PMMCT composite phase change materials

The chemical structure of the phase change material during the preparation process is the basis for its heat storage capability. In this study, PA was absorbed into the porous composite skeleton via the vacuum immersion method for packaging and enhanced the thermal conductivity of the phase change materials. FTIR spectroscopy was used to verify the changes in the chemical structure of PA (Fig. 5a). All of the Ag-PMMCT composite phase change materials show characteristic peaks unique to PA. The characteristic peaks at 2914 and 2847 cm^{-1} are the asymmetric and symmetric bending vibrations of the C–H in the

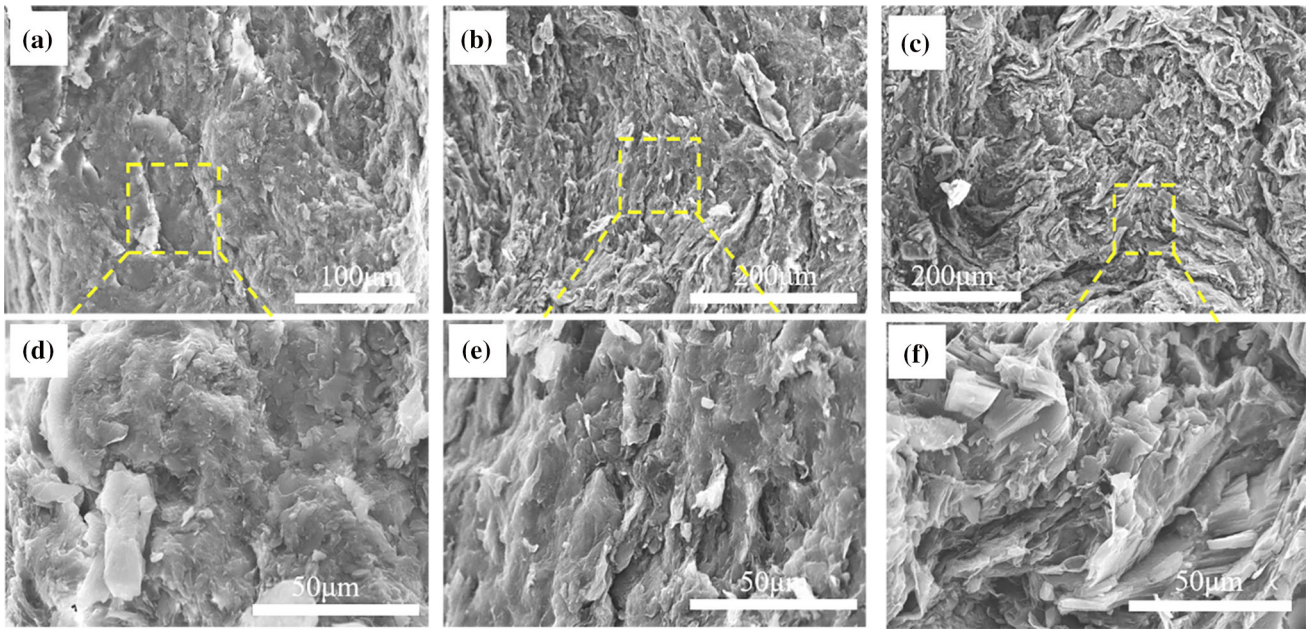

Figure 4 **a**, **b** and **c** SEM images of Ag-PMMCT-1, Ag-PMMCT-3 and Ag-PMMCT-5, respectively. The corresponding enlarged SEM images (**d**, **e** and **f**).

methylene group of the PA. The characteristic peaks at 1693 and 1471 cm^{-1} correspond to the C=O stretching vibration of the carboxyl group and the C–H stretching vibration of the methyl group on the PA, respectively [37]. Furthermore, no new characteristic peaks were observed in the FTIR spectra of the composite, indicating that only physical interactions are involved in the preparation of the Ag-PMMCT composite phase change materials by the vacuum impregnation method. However, due to the relatively small content of the Ag-MMCT porous scaffolds in the Ag-PMMCT composite phase change material, the corresponding characteristic peaks were not observed.

The XRD spectra of the Ag-PMMCT composite phase change materials are shown in Fig. 5. All of the composite phase change materials show distinct diffraction peaks at 21.55° and 24.13°, corresponding to the characteristic diffraction peaks of PA. This indicates that the crystallization behavior of PA in the skeleton remains unchanged. Compared to pure PA, the diffraction peaks of the Ag-PMMCT composite phase change materials were weakened, which was attributed to the interaction of the active functional groups on the MCC, Ag-MWCNT and MXene with the carboxyl groups on the PA; this interaction destroys the original chemical bonding environment of the PA molecule, thereby hindering PA crystallization. Moreover, the diffraction peaks of the MWCNT (100) crystal plane and the Ag (111) crystal plane appeared at 25.6 and 38.1°, respectively, and the intensity of the diffraction peaks gradually weakened with the decrease in the Ag-MWCNT content.

Thermal property analysis of Ag-PMMCT composite phase change materials

The results of the experiments examining the influence of the Ag-MMCT composite scaffold on the thermal storage capacity of PA are shown in Fig. 5c, d. The Ag-MWCNT and MXene in the Ag-PMMCT composite phase change material can accelerate the thermal response of the composite phase change material and promote the melting and crystallization of PA. However, the capillary force and surface adsorption effect of the scaffold micropores will hinder the rotation of the PA molecules. In addition, the active functional groups on the surface of MCC, Ag-MWCNT, and MXene interact with the PA carboxyl groups, hindering the crystallization and melting of PA [38, 39]. As the content of MXene increases, the endothermic peak (Fig. 5c) and exothermic peak (Fig. 5d) of the Ag-PMMCT composite phase change material with MXene are shifted to the high-temperature and low-temperature

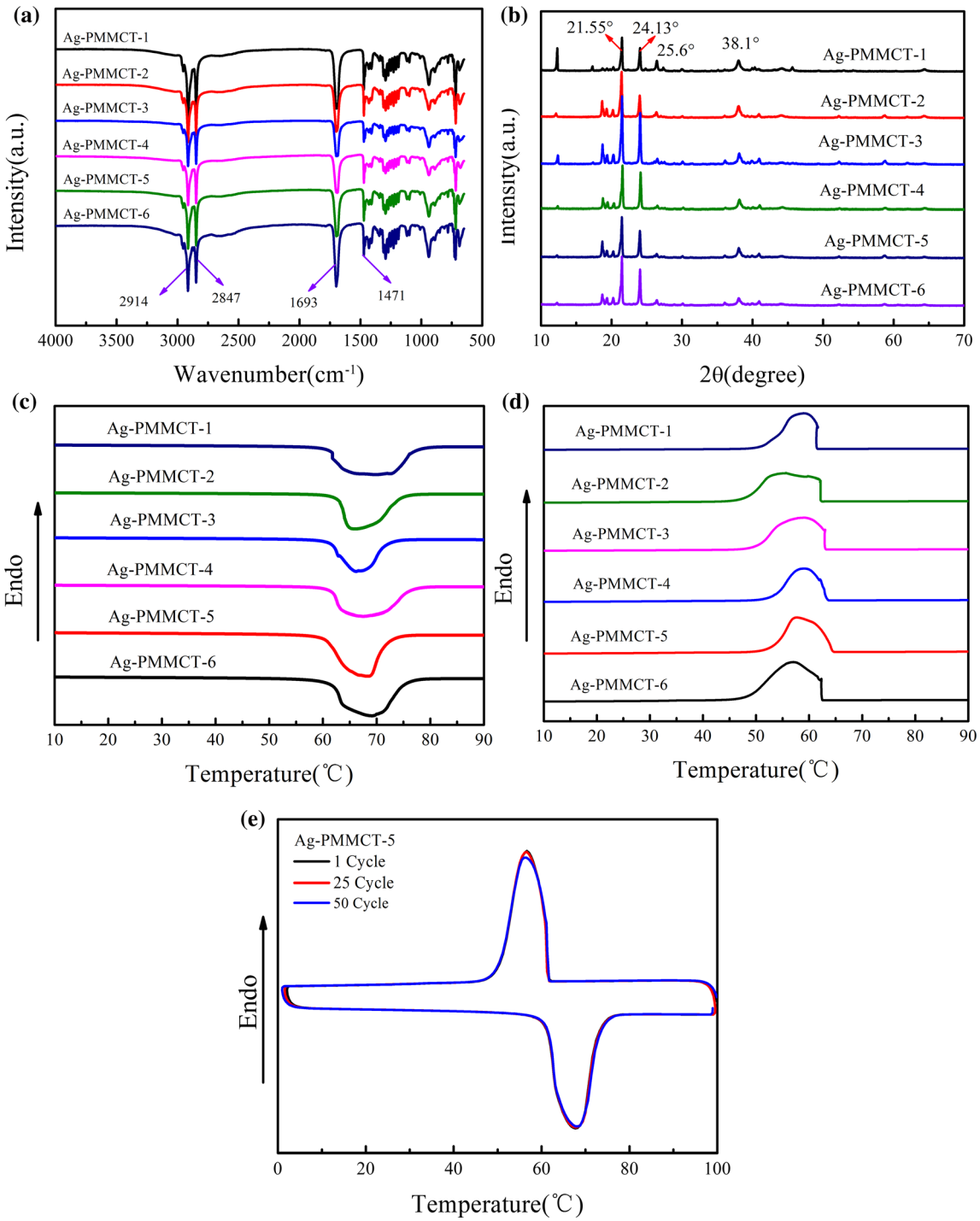

Figure 5 FTIR spectra (**a**), XRD spectra (**b**), the heating (**c**) and cooling (**d**) DSC curves, and DSC cycle diagram of Ag-PMMCT-5 (**e**).

regions, respectively, indicating that the restriction effect of the scaffold in the Ag-PMMCT phase change materials was dominant.

The results for the melting temperature (T_m), latent heat (ΔH_m), crystallization temperature (T_c), and crystallization enthalpy (ΔH_c) of the Ag-PMMCT composite phase change material are shown in Table 1. All of the composite phase change materials show endothermic and crystallization peaks at approximately 66 and 57 °C, respectively, that are closer to the endothermic and exothermic peaks of pure PA. This indicates that only physical

Table 1 Phase transition temperature and corresponding enthalpy value of composite phase change materials

Samples	PA (wt%)	T_m (°C)	ΔH_m (J g^{-1})	T_c (°C)
PA	100	65.21	188.0	59.32
Ag-MMCT-1	86.54	69.10	154.3	56.36
Ag-MMCT-2	86.69	68.78	153.8	55.89
Ag-MMCT-3	86.74	67.59	154.7	57.68
Ag-MMCT-4	86.85	66.26	155.1	58.93
Ag-MMCT-5	86.93	65.49	155.9	57.75
Ag-MMCT-6	86.44	66.76	154.2	59.12

interactions rather than chemical bonding are present between the PA and the Ag-MMCT skeleton, thereby better retaining the original characteristics of the PA. When the amount of the added MXene was 2.92 wt%, a high latent heat of the Ag-PMMCT-6 composite phase change material was obtained (154.2 J g^{-1}) that was only 18% lower than that of pure PA (188.0 J g^{-1}).

The cycle stability of the Ag-PMMCT composite phase change material has a significant impact on its suitability for use in a heat storage system. Taking Ag-PMMCT-5 composite phase change material as a representative, the results for the cycle stability of the composite phase change material are shown in Fig. 5e. After 50 cycles of melting and solidification, the latent heat and enthalpy of crystallization of the Ag-PMMCT-5 composite phase change material are 152.8 and 153.9 J g^{-1}, respectively. These values are essentially unchanged from those in the initial state, indicating that the Ag-PMMCT-5 composite phase change material has good cycle stability for heat storage systems.

The thermal stability of the skeleton and the composite phase change material is also an important factor for the practical application of the material. To determine the thermal stability of the Ag-PMMCT composite phase change material, TG analysis was performed (Fig. 6a, b). The mass loss of the Ag-MMCT porous skeleton before 280 °C was due to the evaporation of adsorbed water, and its decomposition temperature was much higher than the PA phase transition temperature, indicating that it can be applied to PA packaging. Figure 6b shows the changes in the mass of the Ag-PMMCT composite phase change material with temperature. The mass loss of adsorbed water occurs below 200 °C, and the Ag-PMMCT composite phase change material shows almost no evident mass loss, indicating that the Ag-PMMCT composite phase change material was stable and reliable in the phase change temperature range. In addition, as the MXene content increases, the residual carbon rate of the Ag-PMMCT composite phase change material remains unchanged. This was attributed to the good thermal stability of both MXene and Ag-MWCNT under N_2 atmosphere that led to the absence of changes in the total mass of the two materials.

Thermal conductivity analysis of the composite phase change material

The low thermal conductivity of PA is a key factor limiting its wide application. Combining with MXene and Ag-MWCNT synergistically enhances the thermal conductivity of PA. The thermal conductivity of the composite phase change materials in the thickness direction was characterized, and the results for the thermal conductivity of Ag-PMMCT composite phase change materials and its relative PA growth rate are shown in Fig. 6c, d. It is observed that the thermal conductivity of the Ag-PMMCT composite phase change materials was significantly improved by MXene addition (Table S2). For the ratio of MXene to Ag-MWCNT of 1:1, the thermal conductivity of Ag-PMMCT-5 composite phase change material reaches 0.653 W m^{-1} K^{-1}, corresponding to an increase of 202.3% relative to the thermal conductivity of pure PA. This enhancement originates from the two-dimensional structure of MXene and the one-dimensional structure of Ag-MWCNT with high thermal conductivity in the in-plane and along-the-axis directions, respectively [40]. In the composite, the Ag nanoparticles on the MWCNT can serve as a bridge between MWCNT and MXene to form a more ideal heat conduction path [41]. Moreover, the active functional groups (–OH and –COOH) on the surface of MCC, Ag-MWCNT and MXene can interact with the –COOH groups of PA, reducing the interface thermal resistance between the skeleton and PA. However, for the ratio of MXene to Ag-MWCNT of 3:2, the thermal conductivity of Ag-PMMCT-6 composite phase change material was only 0.641 W m^{-1} K^{-1}, corresponding to a decrease by 1.8% relative to that of the Ag-PMMCT-5 composite phase change material. This decrease is due to the agglomeration of the excess MXene layers in the composite scaffold (Fig. 3h).

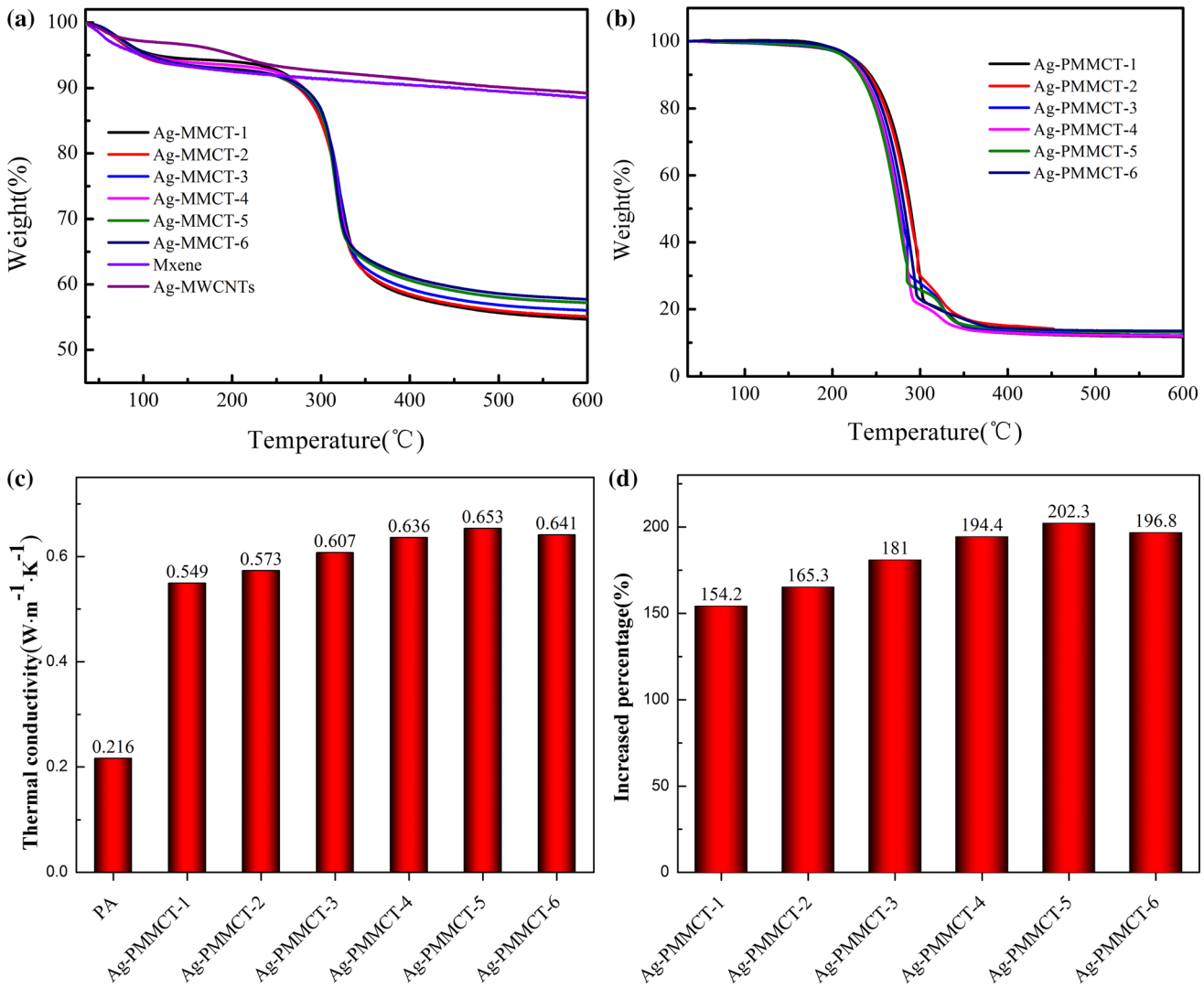

Figure 6 TG curves (**a**) and (**b**), thermal conductivity (**c**) and percent increase in thermal conductivity relative to that of PA (**d**).

Shape stability analysis of composite phase change materials

To explore the packaging effect of the composite scaffold, the PA, Ag-PMMCT-1, Ag-PMMCT-3, Ag-PMMCT-5, and Ag-PMMCT-6 composite phase change materials were continuously heated at 70 °C, and their leakage and shape changes were recorded (Fig. 7a). It was observed that pure PA melts completely after approximately 1 min, and cannot maintain its original shape, while the composite phase change material shows no obvious leakage after heating for 2 h. Additionally, the composite phase change material can still maintain its original shape while supporting a 500 g weight (Fig. 7b), indicating that the composite scaffold has excellent encapsulation and shape stability.

Light-to-heat conversion analysis of composite phase change materials

Composite phase-change heat storage materials for solar thermal utilization require excellent light absorption and light-to-heat conversion capabilities. PA shows weak absorption ability in the ranges of 250–1500 nm as shown in Fig. S2. However, upon the introduction of MXene with excellent optical absorption performance, the Ag-PMMCT composite phase change material shows excellent light absorption, light-to-heat conversion characteristics, and a conversion efficiency of about 70% (Fig. 7c, d and

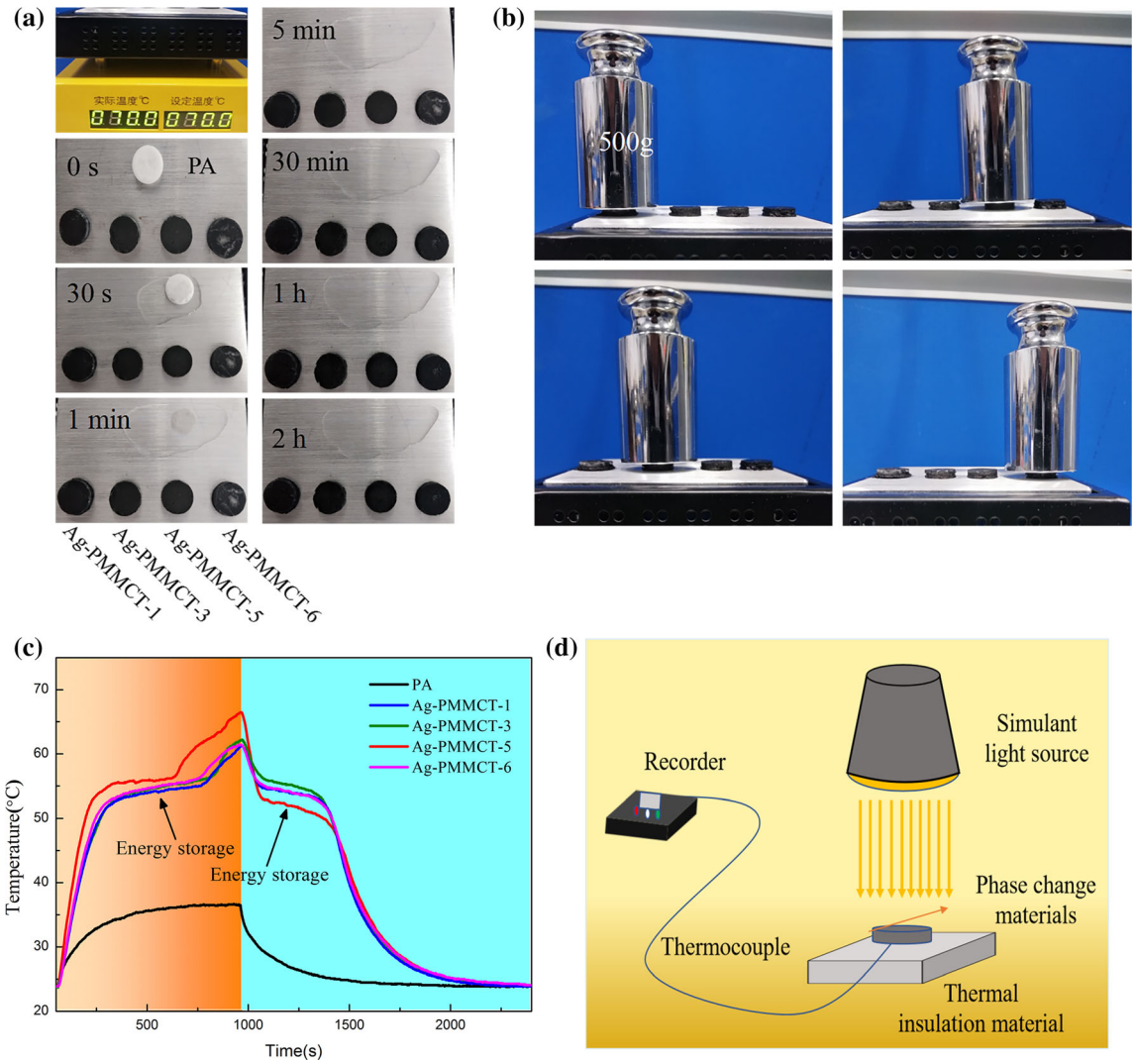

Figure 7 Leakage of composites change materials at 70 °C (**a**), photographs of shape stability (**b**), temperature–time curve of light-to-heat conversion (**c**) and schematic showing light-to-heat conversion experiment (**d**).

Table S3). The lower conversion efficiency of Ag-PMMCT composite phase transition material results from hierarchical pore structure of the composite scaffold and MXene distribution unevenly. Due to the weak photoabsorbtivity of PA, the temperature of PA rises slowly under irradiation with no phase transition throughout the process. The temperature of the Ag-PMMCT composite phase change materials increases rapidly after the irradiation, and the heating rate of the material gradually increased with the increase in the MXene content. For the MXene loading of 2.35%, the phase change of the Ag-PMMCT-5 composite material is observed at 223 s. This is attributed to the enhanced photoabsorption enabled by the higher MXene loading. For the MXene loading of 2.92%, the heating rate of the composite phase change material decreases, which was attributed to the significant agglomeration of the MXene that makes it difficult to form an effective heat conduction path. When the sample temperature rises to the phase change temperature, the heating rate of the phase change material decreases and a plateau appears, indicating that the energy was stored as a latent heat. During the cooling cycle, another plateau appears when the temperature of the composite phase change material decreases to the phase change temperature and the previously stored thermal energy of the phase change material is released to maintain the constant temperature. The photothermal conversion efficiency of Ag-PMMCT composite phase change

material does not show an upward trend with the increase of MXene content, which was attributed to the increased macroporous structure of the composite scaffold with the increased MXene content, increasing the heat transfer barrier and weakening the heat transfer.

Conclusions

Using the synergistic effect of two-dimensional MXene with excellent light-to-heat conversion ability and Ag-MWCNT, the aqueous blend of MCC, MXene, and Ag-MWCNT was crosslinked to prepare a composite hydrogel that was freeze-dried to obtain a porous structure Ag-MMCT composite scaffold. Next, Ag-PMMCT composite phase change materials were prepared via the assisted vacuum impregnation method to absorb palmitic acid. Ag-MWCNT can not only solve the problem of weak interaction between MWCNTs and the matrix, but also compensate for structural defects caused by oxidation of MWCNTs, thereby improving the thermal conductivity of the material. The as-prepared Ag-MMCT composite scaffolds exhibited a typical hierarchical pore structure that provided ample space for PA packaging, and the interpenetrating network structure forms an effective thermal conduction path. The Ag-PMMCT composite phase change material exhibited excellent encapsulation and shape stability, with no obvious leakage after heating 2 h at 70 °C and maintenance of original shape under a load of 500 g. Furthermore, high energy densities of Ag-PMMCT composite phase change materials were still maintained, providing thermal energy storage of 153.8 J g^{-1} and fast light-to-heat energy conversion during the phase change process. In particular, for the MXene to Ag-MWCNT ratio of 1:1, the thermal conductivity of the composite phase change material was 0.653 W m^{-1} K^{-1}, corresponding to an increase of 202.3% relative to that of pure PA. Therefore, the Ag-PMMCT composite phase change materials can be further used in energy conversion and storage systems and in thermal management of devices and electronics.

Associated content

Supporting information

Pore size distribution and composition of Ag-MMCT composite scaffolds, UV–vis-NIR absorption, thermal conductivity, photothermal conversion efficiency, and percent increase in thermal conductivity relative to that of PA of Ag-PMMCT materials.

Acknowledgements

The authors are grateful for generous financial support provided by the National Natural Science Foundation of China (grant number 52063006) and the Science and technology Foundation of Guizhou Province (grant number 2019-112-016).

Declarations

Conflict of interest The authors declare that they have no conflict of interest.

Supplementary Information: The online version contains supplementary material available at https://doi.org/10.1007/s10853-021-06659-7.

References

[1] Nazir H, Batool M, Osorio FJB, Isaza-Ruiz M, Xu X, Vignarooban K, Phelan P, Inamuddin KAM (2019) Recent developments in phase change materials for energy storage applications: a review. Int J Heat Mass Tran 129:491–523. https://doi.org/10.1016/j.ijheatmasstransfer.2018.09.126

[2] Kalidasan B, Pandey AK, Shahabuddin S, Samykano M, Thirugnanasambandam M, Saidur R (2020) Phase change materials integrated solar thermal energy systems: global trends and current practices in experimental approaches. J Energy Storage 27. https://doi.org/10.1016/j.est.2019.101118

[3] Su W, Darkwa J, Kokogiannakis G (2017) Development of microencapsulated phase change material for solar thermal energy storage. Appl Therm Eng 112:1205–1212. https://doi.org/10.1016/j.applthermaleng.2016.11.009

[4] Sharifi NP, Shaikh AAN, Sakulich AR (2017) Application of phase change materials in gypsum boards to meet building energy conservation goals. Energy Buildings 138:455–467. https://doi.org/10.1016/j.enbuild.2016.12.046

[5] Krishna J, Kishore PS, Solomon AB (2017) Heat pipe with nano enhanced-PCM for electronic cooling application. Exp Therm Fluid Sci 81:84–92. https://doi.org/10.1016/j.expthermflusci.2016.10.014

[6] Shaid A, Wang L, Islam S, Cai JY, Padhye R (2016) Preparation of aerogel-eicosane microparticles for thermoregulatory coating on textile. Appl Therm Eng 107:602–611. https://doi.org/10.1016/j.applthermaleng.2016.06.187

[7] Xia M, Yuan Y, Zhao X, Cao X, Tang Z (2016) Cold storage condensation heat recovery system with a novel composite phase change material. Appl Energ 175:259–268. https://doi.org/10.1016/j.apenergy.2016.05.001

[8] Zhong Y, Zhou M, Huang F, Lin T, Wan D (2013) Effect of graphene aerogel on thermal behavior of phase change materials for thermal management. Sol Energ Mat Sol C 113:195–200. https://doi.org/10.1016/j.solmat.2013.01.046

[9] Yang L, Jin X, Zhang Y, Du K (2021) Recent development on heat transfer and various applications of phase-change materials. J Clean Prod 287. https://doi.org/10.1016/j.jclepro.2020.124432

[10] Pielichowska K, Pielichowski K (2014) Phase change materials for thermal energy storage. Prog Mater Sci 65:67–123. https://doi.org/10.1016/j.pmatsci.2014.03.005

[11] Ma G, Liu S, Xie S, Jing Y, Zhang Q, Sun J, Jia Y (2017) Binary eutectic mixtures of stearic acid-n-butyramide/n-octanamide as phase change materials for low temperature solar heat storage. Appl Therm Eng 111:1052–1059. https://doi.org/10.1016/j.applthermaleng.2016.10.004

[12] Zhang GH, Yu ZJ, Cui GM, Dou BL, Lu W, Yan XY (2020) Fabrication of a novel nano phase change material emulsion with low supercooling and enhanced thermal conductivity. Renew Energ 151:542–550. https://doi.org/10.1016/j.renene.2019.11.044

[13] Milian YE, Gutierrez A, Grageda M, Ushak S (2017) A review on encapsulation techniques for inorganic phase change materials and the influence on their thermophysical properties. Renew Sust Energ Rev 73:983–999. https://doi.org/10.1016/j.rser.2017.01.159

[14] Nirwan A, Kumar R, Mondal B, Kumar J, Bera A, Kumar R (2020) Thermal performance assessment of lauric acid and palmitic acid based multi-transformation phase change material and exfoliated graphite composites. Energ Source A 10(1080/15567036):1818004

[15] Wang C, Feng L, Li W, Zheng J, Tian W, Li X (2012) Shape-stabilized phase change materials based on polyethylene glycol/porous carbon composite: the influence of the pore structure of the carbon materials. Sol Energ Mat Sol C 105:21–36. https://doi.org/10.1016/j.solmat.2012.05.031

[16] Xiong W, Mehrabadi BAT, Karakolos SG, White RD, Shakouri A, Kasak P, Zaidi SJ, Weidner JW, Regalbuto JR, Colon-Mercado H, Monnier JR (2020) enhanced performance of oxygen-functionalized multiwalled carbon nanotubes as support for Pt and Pt–Ru bimetallic catalysts for methanol electrooxidation. ACS Appl Energ Mater 3(6):5487–5496. https://doi.org/10.1021/acsaem.0c00477

[17] Zhu TY, Liu SL, Wan KN, Zhang C, Feng YY, Feng W, Liu TX (2020) Fluorine and nitrogen dual-doped porous carbon nanosheet-enabled compact electrode structure for high volumetric energy storage. ACS Appl Energ Mater 3(5):4949–4957. https://doi.org/10.1021/acsaem.0c00500

[18] Xiao D, Qu Y, Hu S, Han H, Li Y, Zhai J, Jiang Y, Yang H (2015) Study on the phase change thermal storage performance of palmitic acid/carbon nanotubes composites. Compos A-Appl S 77:50–55. https://doi.org/10.1016/j.compositesa.2015.06.020

[19] Xu B, Li Z (2014) Paraffin/diatomite/multi-wall carbon nanotubes composite phase change material tailor-made for thermal energy storage cement-based composites. Energy 72:371–380. https://doi.org/10.1016/j.energy.2014.05.049

[20] Li M, Chen M, Wu Z (2014) Enhancement in thermal property and mechanical property of phase change microcapsule with modified carbon nanotube. Appl Energ 127:166–171. https://doi.org/10.1016/j.apenergy.2014.04.029

[21] Zhang X, Wang X, Lei Z, Wang L, Tian M, Zhu S, Xiao H, Tang X, Qu L (2020) Flexible MXene-decorated fabric with interwoven conductive networks for integrated joule heating, electromagnetic interference shielding, and strain sensing performances. ACS Appl Mater Inter 12(12):14459–14467. https://doi.org/10.1021/acsami.0c01182

[22] He NF, Patil S, Qu JG, Liao JY, Zhao F, Gao W (2020) effects of electrolyte mediation and MXene size in fiber-shaped supercapacitors. ACS Appl Energ Mate 3(3):2949–2958. https://doi.org/10.1021/acsaem.0c00024

[23] Liu X, Jin X, Li L, Wang J, Yang Y, Cao Y, Wang W (2020) Air-permeable, multifunctional, dual-energy-driven MXene-decorated polymeric textile-based wearable heaters with exceptional electrothermal and photothermal conversion performance. J Mater Chem A 8(25):12526–12537. https://doi.org/10.1039/d0ta03048a

[24] Fan X, Ding Y, Liu Y, Liang J, Chen Y (2019) Plasmonic $Ti_3C_2T_X$ MXene enables highly efficient photothermal conversion for healable and transparent wearable device. ACS Nano 13(7):8128134. https://doi.org/10.1021/acsnano.9b03161

[25] Li R, Zhang L, Shi L, Wang P (2017) MXene Ti_3C_2: an effective 2D light-to-heat conversion material. ACS Nano 11(4):3752–3759. https://doi.org/10.1021/acsnano.6b08415

[26] Du X, Qu J, Deng S, Du Z, Cheng X, Wang H (2020) $Ti_3C_2T_x$@PDA-integrated polyurethane phase change composites with superior solar-thermal conversion efficiency and improved thermal conductivity. ACS Sustain Chem Eng 8(14):5799–5806. https://doi.org/10.1021/acssuschemeng.0c01582

[27] Fan X, Liu L, Jin X, Wang W, Zhang S, Tang B (2019) MXene $Ti_3C_2T_x$ for phase change composite with superior photothermal storage capability. J Mater Chem A 7(23):14319–14327. https://doi.org/10.1039/c9ta03962g

[28] Tang L, Zhao X, Feng C, Bai L, Yang J, Bao R, Liu Z, Yang M, Yang W (2019) Bacterial cellulose/MXene hybrid aerogels for photodriven shape-stabilized composite phase change materials. Sol Energ Mat Sol C, 203. https://doi.org/10.1016/j.solmat.2019.110174

[29] Chiang IW, Brinson BE, Smalley RE, Margrave JL, Hauge RH (2012) Purification and characterization of single-wall carbon nanotubes. J Phys Chem B 105(6):1157–1161. https://doi.org/10.1021/jp003453z

[30] Yan D, Wang F, Zhao Y, Liu J, Wang J, Zhang L, Park KC, Endo M (2009) Production of a high dispersion of silver nanoparticles on surface-functionalized multi-walled carbon nanotubes using an electrostatic technique. Mater Lett 63(2):171–173. https://doi.org/10.1016/j.matlet.2008.09.018

[31] Aftab W, Mahmood A, Guo WH, Yousaf M, Tabassum H, Huang XY, Liang ZB, Cao AY, Zou RQ (2019) Polyurethane-based flexible and conductive phase change composites for energy conversion and storage. Energy Storage Mater 20:401–409. https://doi.org/10.1016/j.ensm.2018.10.014

[32] Sheng X, Zhao Y, Zhang L, Lu X (2019) Properties of two-dimensional Ti_3C_2 MXene/thermoplastic polyurethane nanocomposites with effective reinforcement via melt blending. Compos Sci Technol 181. https://doi.org/10.1016/j.compscitech.2019.107710

[33] Luo J, Tao X, Zhang J, Xia Y, Huang H, Zhang L, Gan Y, Liang C, Zhang W (2016) Se^{4+} Ion decorated highly conductive Ti_3C_2 MXene: promising lithium-ion anodes with enhanced volumetric capacity and cyclic performance. ACS Nano 10(2):2491–2499. https://doi.org/10.1021/acsnano.5b07333

[34] Wang D, Lin Y, Hu D, Jiang P, Huang X (2020) Multifunctional 3D-MXene/PDMS nanocomposites for electrical, thermal and triboelectric applications. Compos A-Appl S 130. https://doi.org/10.1016/j.compositesa.2019.105754

[35] Sun H, Xu Z, Gao C (2013) Multifunctional, ultra-flyweight, synergistically assembled carbon aerogels. Adv Mater 25(18):2554–2560. https://doi.org/10.1002/adma.201204576

[36] Mehrali M, Latibari ST, Mehrali M, Mahlia TMI, Sadeghinezhad E, Metselaar HSC (2014) Preparation of nitrogen-doped graphene/palmitic acid shape stabilized composite phase change material with remarkable thermal properties for thermal energy storage. Appl Energ 135:339–349. https://doi.org/10.1016/j.apenergy.2014.08.100

[37] Mishra AK, Lahiri BB, Solomon V, Philip J (2019) Nano-inclusion aided thermal conductivity enhancement in palmitic acid/di-methyl formamide phase change material for latent heat thermal energy storage. Thermochim Acta 678. https://doi.org/10.1016/j.tca.2019.178309

[38] Yang J, Li X, Han S, Yang R, Min P, Yu Z-Z (2018) High-quality graphene aerogels for thermally conductive phase change composites with excellent shape stability. J Mater Chem A 6(14):5880–5886. https://doi.org/10.1039/c8ta00078f

[39] Yang J, Li X, Han S, Zhang Y, Min P, Koratkar N, Yu Z-Z (2016) Air-dried, high-density graphene hybrid aerogels for phase change composites with exceptional thermal conductivity and shape stability. J Mater Chem A 4(46):18067–18074. https://doi.org/10.1039/c6ta07869a

[40] Liang X, Cheng Q (2018) Synergistic reinforcing effect from graphene and carbon nanotubes. Compos Commun 10:122–128. https://doi.org/10.1016/j.coco.2018.09.002

[41] Zeng X, Yao Y, Gong Z, Wang F, Sun R, Xu J, Wong C-P (2015) Ice-templated assembly strategy to construct 3D boron nitride nanosheet networks in polymer composites for thermal conductivity improvement. Small 11(46):6205–6213. https://doi.org/10.1016/j.coco.2020.100601